Certification of Standard Reference Material 660c for powder diffraction

David R. Black,[1,a] Marcus H. Mendenhall,[1] Craig M. Brown,[2] Albert Henins,[1] James Filliben,[3] and James P. Cline[1]

[1]*Materials Measurement Science Division of Material Measurement Laboratory, National Institute of Standards and Technology, Gaithersburg, Maryland 20899, USA*

[2]*Center for Neutron Research, National Institute of Standards and Technology, Gaithersburg, Maryland 20899, USA*

[3]*Statistical Engineering Division, National Institute of Standards and Technology, Gaithersburg, Maryland 20899, USA*

(Received 17 December 2019; accepted 15 January 2020)

The National Institute of Standards and Technology (NIST) certifies a suite of Standard Reference Materials (SRMs) to evaluate specific aspects of instrument performance of both X-ray and neutron powder diffractometers. This report describes SRM 660c, the fourth generation of this powder diffraction SRM, which is used primarily for calibrating powder diffractometers with respect to line position and line shape for the determination of the instrument profile function (IPF). It is certified with respect to lattice parameter and consists of approximately 6 g of lanthanum hexaboride (LaB_6) powder. So that this SRM would be applicable for the neutron diffraction community, the powder was prepared from an isotopically enriched ^{11}B precursor material. The microstructure of the LaB_6 powder was engineered specifically to yield a crystallite size above that where size broadening is typically observed and to minimize the crystallographic defects that lead to strain broadening. A NIST-built diffractometer, incorporating many advanced design features, was used to certify the lattice parameter of the LaB_6 powder. Both Type A, statistical, and Type B, systematic, uncertainties have been assigned to yield a certified value for the lattice parameter at 22.5 °C of $a = 0.415\ 682\ 6 \pm 0.000\ 008$ nm (95% confidence). [doi:10.1017/S0885715620000068]

Key words: certification, diffractometer, lattice parameter, Standard Reference Material, X-ray diffraction

I. INTRODUCTION

The laboratory-based divergent-beam X-ray diffractometer can provide a wealth of structural and microstructural information about a wide variety of materials. However, to successfully collect and interpret the data, the operator must have both a properly aligned instrument and take into consideration the aberrations inherent to the para-focusing optics. One method to accomplish this is to use standards to evaluate instrument performance. The National Institute of Standards and Technology (NIST) certifies a suite of Standard Reference Materials (SRMs) to address specific aspects of powder diffractometer performance. This report describes SRM 660c, the fourth generation of this powder diffraction standard, which is certified with respect to lattice parameter. It consists of approximately 6 g of lanthanum hexaboride (LaB_6) powder specifically prepared to have minimal line broadening. It is commonly used for determination of the instrument contribution to the observed line profile, the instrument profile function (IPF), and calibrating powder diffractometers with respect to line position.

II. MATERIAL

The lanthanum hexaboride feedstock for SRM 660c was manufactured for NIST with a dedicated processing run (H.C Starck GmbH, Goslar, Germany, now Höganäs AB, SE-263 83 Höganäs, Sweden). (Certain commercial equipment, instruments, or materials are identified in this in order to adequately specify the experimental procedure. Such an identification does not imply recommendation or endorsement by NIST, nor does it imply that the materials or equipment identified are necessarily the best available for the purpose.) One of the precursor materials, boron carbide, was isotopically enriched with the ^{11}B isotope to a nominal concentration of 99% (Ceradyne Boron Products LLC, Quapaw, OK, USA, now Ceradyne, Inc., a 3M company). The ^{10}B isotope has a neutron capture coefficient nearly six orders of magnitude larger than ^{11}B and at the naturally occurring abundance of nearly 20% results in extremely high neutron absorption, rendering a lanthanum hexaboride made from it essentially opaque to neutrons and therefore not applicable to diffraction experiments. The use of the ^{11}B isotope eliminates this problem and yields an SRM that is relevant to both the X-ray and neutron diffraction communities. Estimates of the actual ^{10}B content and bulk powder transmission properties were derived from small-angle neutron scattering (SANS) experiments as

[a]Author to whom correspondence should be addressed. Electronic mail: david.black@nist.gov

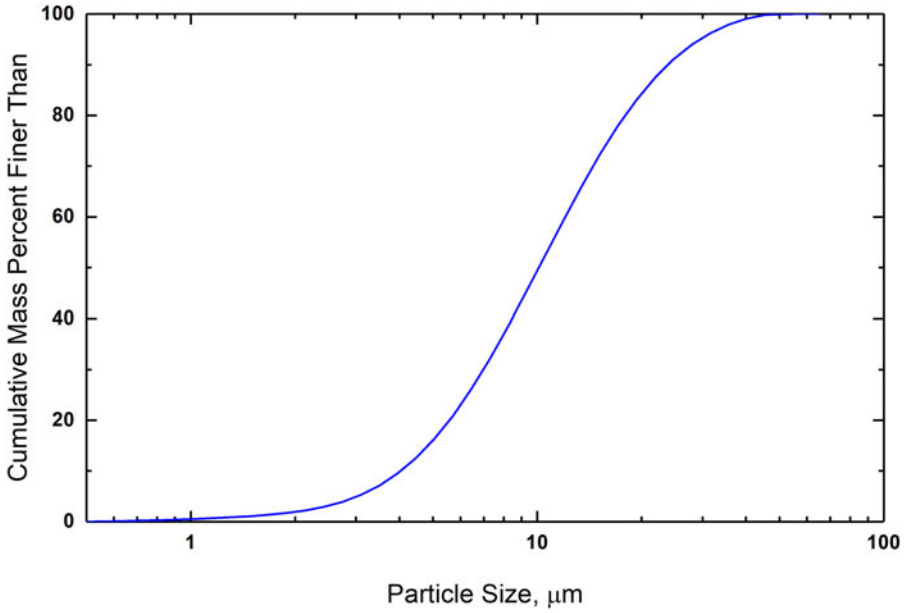

Figure 1. (Colour online) Particle size distribution of lanthanum hexaboride feedstock.

will be described later. The LaB_6 powder was annealed at 1700 °C under argon for 1 h in an induction furnace to remove crystallographic defects and grow the crystallites to minimize sample-induced broadening (Cerac Inc., Milwaukee, WI, USA, now Materion Corporation). The powder sintered to a small extent during the annealing process and, therefore, was lightly ground in a mortar and pestle and passed through a 44 μm sieve to remove any remaining large particles. Figure 1 shows typical particle size data from laser scattering measurements. Each individual unit of SRM 660c was bottled under argon gas.

III. EXPERIMENT

X-ray powder diffraction data were collected on a NIST-built diffractometer that incorporates several advanced design features, such as high accuracy optical encoders and temperature control <0.1 K. A full discussion of this instrument, its alignment and calibration can be found in Cline *et al.* (2015, 2019). The optical layout is that of a conventional Bragg-Brentano divergent-beam diffractometer, utilizing a Cu X-ray source, a sample spinner, a graphite post-sample monochromator, and a scintillation detector. Linkage to the International System of Units (SI) (BIPM, 2006) is established via the emission spectrum of Cu$K\alpha$ radiation, which forms the basis for constructing the diffraction profiles in the fundamental parameters approach (FPA) method of data analysis (Cheary and Coelho, 1992). The models for the geometric component of the profiles included source and receiving slit width, flat specimen error and axial divergence. Rigorous analysis of data from this divergent-beam diffractometer requires knowledge of both the diffraction angle and the effective source–sample–detector distances. Therefore, two additional models, specimen displacement and X-ray attenuation, must be included in the data analysis as these factors affect the distances critical in the use of this experimental geometry. Data were analyzed in the context of both Type A uncertainties, assigned by statistical analysis, and Type B uncertainties, based on knowledge of the nature of systematic errors in the measurements, to result in the establishment of robust uncertainties for the certified values (Taylor and Kuyatt, 1994; JCGM 100, 2008).

A random stratified selection process was used to extract ten bottles of SRM 660c from a total population of 1096 bottles in stock. Two samples were prepared from each bottle, for a total of 20 samples. Certification data sets were collected from 24 regions of the diffraction pattern, with each region including only one of the 24 allowed reflections accessible within the diffractometer 2θ range of 20°–150°. The scan parameters for each peak are given in Table I. The angular width of each region was selected to be approximately 15 times the observed full-width at half-maximum (FWHM) of the profile, and the step width was chosen to include at least eight data points above the FWHM. The dwell time for each profile was inversely proportional to the observed diffraction intensity and calculated, so that the total collection time for each sample was about 22 h. Certification data were recorded with the X-ray tube operating at an accelerating voltage of 45 kV and a current of 40 mA. The source size was approximately 12 mm × 0.04 mm, and the goniometer radius was 217.5 mm. The divergence slit was nominally set to 0.8°, so that at the lowest θ angle, the projected size of the source was just less than the sample size. Samples were spun, about the normal to their surface, at 0.5 Hz during data collection. A Soller slit with a divergence of 2.2° further defined the incident beam in the axial direction. A 2 mm anti-scatter slit was placed approximately 113 mm in front of the receiving slit of 0.2 mm (0.05°). The source was allowed to equilibrate at operating conditions for at least an hour prior to collecting any data, and samples were selected for data collection in a random order. The temperature and humidity within the diffractometer enclosure were recorded during data collection using Veriteq SP 2000 monitors with a stated accuracy of ±0.15 K. The variation in temperature over the course of any scan was typically less than 0.1 K.

In order to assess the crystallite size of SRM 660c, several data sets were collected at the Advanced Photon Source (APS) on the 11-BM high-resolution powder diffractometer (Wang *et al.*, 2008). The resolution of this machine is sufficiently

https://doi.org/10.1017/S0885715620000068 Published online by Cambridge University Press

TABLE I. Run time parameters for the data collection from SRM 660c.

hkl	Start angle (°)	End angle (°)	Step width (°)	Count time (s)	Total peak time (min)
100	20.3	22.2	0.01	2	6.3
110	29.1	31.4	0.01	1	3.8
111	36.4	38.4	0.01	3	10
200	42.7	44.4	0.01	5	14.2
210	48	50	0.008	2	8.3
211	53.2	54.896	0.008	5	17.7
110	62.5	64.204	0.008	11	39
300	66.7	68.596	0.008	4	15.8
310	70.9	72.7	0.008	6	22.5
311	75	76.904	0.008	9	35.7
222	79.3	80.804	0.008	47	147.3
320	83	84.904	0.008	15	59.5
321	86.9	88.9	0.008	8	33.3
400	95	96.704	0.008	42	149.1
410	98.6	100.8	0.008	9	41.3
330	102.7	104.9	0.008	12	55
331	106.9	108.9	0.01	27	90
420	111.1	113.1	0.01	20	66.7
421	115.3	117.6	0.01	10	38.3
332	119.9	122.1	0.01	19	69.7
422	129.6	131.796	0.012	32	97.6
500	134.9	137.396	0.012	27	93.6
510	140.5	144	0.014	7	29.2
511	147.5	150.908	0.016	15	53.2

high that a credible analysis of the crystallite size broadening of the LaB_6 could be performed. TOPAS (Bruker, 2017) was used to analyze the data using the FPA method with Pawley fits to the data (Pawley, 1981). Included in the refinements was a parameter for Lorentzian broadening varying as $1/\cos\theta$ interpreted as crystallite size-induced broadening. This resulted in a volume-weighted mean crystallite size, $\langle L\rangle_{vol}$, of 500 nm, based on an assumption of spherical crystallites. This degree of crystallite size broadening is undetectable on laboratory X-ray equipment.

A bottle was chosen at random to determine the neutron transmission for a cylindrical vanadium cell of 6 mm internal diameter commonly used for neutron powder diffraction measurements. The packing density of the powder was determined from the mass of powder in a known volume that was tapped in a similar fashion as the sample in the vanadium cell (1.08 g cm^{-3}). The NG-7 SANS instrument at the NIST Center for Neutron Research was configured for standard transmission measurement with an aperture in a Cd mask placed in front of the sample that was 4 mm wide and 15 mm tall. The SANS instrument was configured with 15.3 m sample-to-detector distance, 8 guides inserted, and 4 attenuators. A velocity selector is used to provide a wavelength of 6 Å with $\Delta\lambda/\lambda$ of ≈15%. The direct beam covers approximately 40 pixels × 50 pixels on the detector. The counting time for an empty vanadium cell and one filled with $La^{11}B_6$ were 180 s each with a nominal neutron flux of 6.6×10^6 n cm^{-2} s^{-1}.

The ratio of integrated neutron detector counts for the $La^{11}B_6$ in the vanadium cell to that of the empty vanadium cell at a wavelength of 6 Å results in a transmission of 17.2%. Using the estimated packing density, we calculate (NCNR, 2019) an approximate isotopic purity of 98.8% ^{11}B, close to the nominal 99% given from the manufacturer. For a neutron wavelength of 1.54 Å, the calculated transmission is 63%, within the range commonly used for crystallography measurements. To improve the transmission to 90% at this wavelength, we calculate that an isotopic purity of 99.9975% ^{11}B is needed.

IV. DATA ANALYSIS

The certification data were analyzed using the FPA method with a Rietveld refinement as implemented in TOPAS. A NIST developed Python-based code that implements the FPA method (Mendenhall *et al*., 2015) was also used in a Pawley analysis. With the Python-based code, the 20 data sets from SRM 660c were analyzed simultaneously in a global refinement. This approach allowed the analysis of specific parameters of the IPF to be carried out in the context of highly favorable Poisson counting statistics. The analysis used the energy of the Cu$K\alpha$ emission spectrum as characterized by Hölzer *et al*. (1997) and included a satellite component (Maskil and Deutsch, 1988) and the "tube tails" (Bergmann *et al*., 2000). However, as reported by Cline *et al*. (2015), the graphite post-monochromator imposes a bandpass on the diffracted beam that reduces the apparent breadth of the Cu$K\alpha$ emission spectrum from the values reported by Hölzer by approximately 20%. Therefore, it was desired to refine the breadth with a global refinement to realize the benefits of the favorable Poisson counting statistics.

In the global refinement, parameters specific to each sample, such as displacement and attenuation terms, were allowed to refine independently. While parameters specific to either SRM 660c, such as the lattice parameter, or the instrument, were constrained to a single, refined value. The breadths of the four Lorentzian profiles used to describe the Cu$K\alpha$ emission spectrum were refined in order to assess the impact of the post-monochromator. In these analyses, the FWHM values of the two pairs of profiles in the emission spectrum were constrained, $K\alpha_{11}$ with $K\alpha_{12}$ and $K\alpha_{21}$ with $K\alpha_{22}$, to preserve the overall shape as reported by Hölzer. This refinement included the intensities and positions of the satellite lines and the "tube tails". A Soller slit value, constrained to be identical for both the incident and diffracted beam, using the "full" axial divergence model (Cheary and Coelho, 1998a, 1998b), was also refined. In this manner, highly credible values for parameters specific to the IPF were obtained and fixed for subsequent refinements to obtain the certified lattice parameters. Additionally, the IPF parameters obtained from fits to individual data sets essentially duplicated those of the global approach.

The IPF parameters obtained with the global fit were used in the Rietveld analyses using TOPAS. The refined parameters included the scale factors, Chebyshev polynomial terms for modeling of the background, the lattice parameters, specimen displacement and attenuation terms, structural parameters and a term for Lorentzian size broadening. With these analyses, the refinements were performed on the individual scans resulting in 20 values for the lattice parameter that were used to obtain the certified values. The goodness of fit parameter was about 1.3. The lattice parameter obtained from the Python-based FPA global refinement and the average of the 20 values obtained individually from the TOPAS FPA analysis agreed to within 2 fm. This lends credibility to the premise that both codes are working in correspondence to published FPA models. The refined lattice parameters were adjusted using the coefficient of thermal expansion values found in

https://doi.org/10.1017/S0885715620000068 Published online by Cambridge University Press

TABLE II. Certification data for SRM 660c.

Bottle number	Lattice parameter (nm)
1000a	0.415 682 980
300b	0.415 682 529
200a	0.415 681 952
600a	0.415 682 704
900b	0.415 682 519
800b	0.415 681 859
700b	0.415 683 599
600b	0.415 682 989
500b	0.415 682 854
400a	0.415 683 519
400b	0.415 682 434
500a	0.415 683 869
1000b	0.415 681 637
700a	0.415 682 927
900a	0.415 681 557
200b	0.415 682 392
100b	0.415 682 577
800a	0.415 681 942
100a	0.415 682 024
300a	0.415 683 429

Sirota *et al*. (1998) to values at 22.5 °C and are given in Table II.

The efficacy of the FPA models can be evaluated by examining the variation in refined lattice parameter as a function of 2θangle. This variation is due primarily to the asymmetry of the X-ray line profiles which varies in both the degree and direction over the full 2θ range. This is illustrated in Figure 2, wherein the left (low-angle side) and right (high-angle side) half-width at half-maximum (HWHM) of the line profiles are shown as a function of 2θ angle. These values were obtained by fitting individual peaks of the certification data with a split pseudo-Voigt profile shape function with unity weighting (Cline *et al*., 2015). The angular dispersion, $d\theta/d\lambda$, will result in increasing FWHM values with tanθ, as is apparent in the data of Figure 2. Furthermore, the discontinuity observed for the (100) peak at 21.4° is due to low angular dispersion at this angle and the apparent "merging" of the contributions of the copper $K\alpha_1$ and $K\alpha_2$ lines; this biases the profile fitting procedure to yield nonphysical results. Axial divergence broadens the peaks to the low-angle side below ≈110°, and to the high-angle side above this value (Cheary and Coelho, 1998a, 1998b), as illustrated in Figure 2. The effects of the incident beam slit will also asymmetrically broaden the low-angle lines to the low-angle side. Thus, the region of minimal FWHM values is observed to be 40°–70°, while the region of minimal asymmetry will be 90°–120°; both effects are in conjunction with expectations.

The use of the FPA for the fitting of X-ray line profiles generally entails the refinement of models across the full 2θ range; this ensures the most accurate representation of the various contributions to the observed line shape. If the FPA model was working "perfectly", i.e., faithfully representing all physical parameters of the instrument, the lattice parameters obtained from FPA fits to the individual profiles would be uniform with respect to diffraction angle. To examine this behavior, the optimum IPF parameters obtained by the global FPA fit to the 20 data sets using the Python-based code were used. These values were then fixed, and the lattice parameter of each peak then refined independently, permitting optimization in 2θ space alone, yielding 24 lattice parameter values for each scan. Figure 3 illustrates the difference between the single lattice parameter obtained with the global Pawley fit and those obtained with fits to the individual profiles. This plot can be considered in the context of Bragg's law, diffraction optics, and the properties of nonlinear least-squares fitting. Dispersion in d with respect to θ, $d(d)/d(\theta)$, follows 1/tanθ; hence, the high sensitivity of d values at lower 2θ angles. The symmetric, broad peaks in the 90°–120° region effectively anchor the refined lattice parameter due to their relative independence on the model and small values of 1/tanθ. The peaks in the 40°–70° range also anchor the lattice parameter as they are intrinsically narrow and are only affected by modest values of 1/tanθ. It is observed that the scatter in the data points above 40° in Figure 3 is relatively modest reflecting a reduced uncertainty in the reported values. This is in sharp contrast to the low-angle lines which are adversely affected by both the axial divergence and a large 1/tanθ dependence. These low-angle peaks display a larger scatter in their values. While we do not show formal error

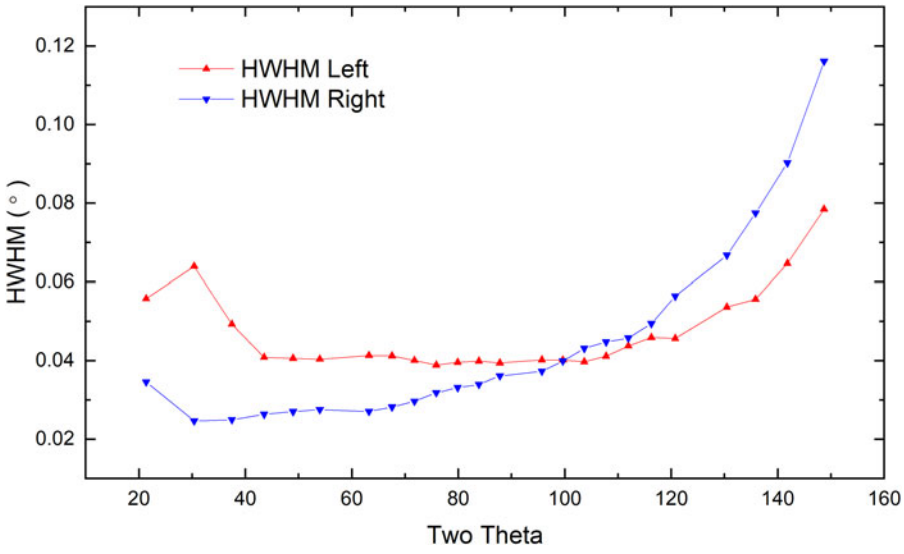

Figure 2. (Colour online) Left and right HWHM values obtained via a refinement using a split pseudo-Voigt profile shape function with unity weighting.

https://doi.org/10.1017/S0885715620000068 Published online by Cambridge University Press

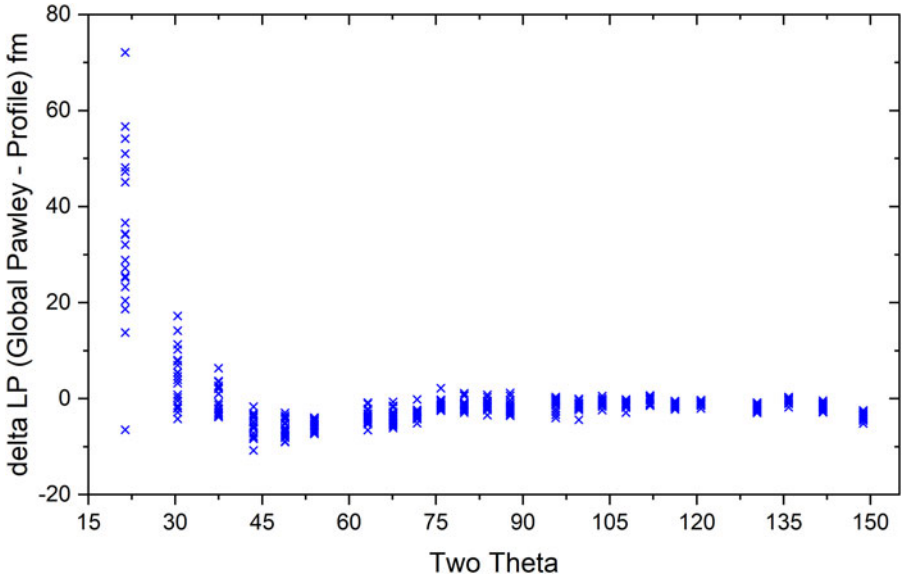

Figure 3. (Colour online) Lattice parameter difference between the value obtained via a global FPA Pawley analysis vs. values obtained via the refinement of individual profile position with the FPA parameters frozen at the global values.

values (σ) derived from the variance–covariance matrix, the large scatter of the low-angle points is nonetheless consistent with the large σ associated with these values. Since the contribution of points to χ^2, which is minimized in least-squares fitting, is inversely weighted by the σ^2 from the variance–covariance matrix, the large uncertainty at low angles implies that these points have very little effect on the final fit values.

A statistical analysis of the data indicated that the mean of the measurements was $a = 0.415\ 682\ 6$ nm with a $k = 2$ Type A expanded uncertainty of 0.000 000 37 nm. However, a Type B uncertainty due to systematic uncertainty must be incorporated into the uncertainty bounds of the certified lattice parameter. While every effort has been taken to understand and take into account the nature of the uncertainties in the experimental procedure and in the data analysis process, unspecified uncertainties certainly exist. Insight into the magnitude of possible systematic uncertainties can be gained by examining Figure 3. As discussed above, the large scatter of the low-angle data results from well-understood causes and as such they do not contribute to an understanding of additional systematic uncertainty. Except for a single value, all data for the peaks between 40° and 120°, which includes the range of both minimum FWHM and highest symmetry, fall between ±8 fm. This leads to an assignment of a Type B expanded uncertainty (95% confidence) of ± 0.000 008 nm and a final certified lattice parameter of $a = 0.415\ 682\ 6 \pm 0.000008$ nm.

V. CONCLUSION

A NIST-built divergent-beam diffractometer, incorporating many advanced design features, has been used to certify the lattice parameter of LaB_6 powder for SRM 660c. The powder was specifically prepared to minimize the effects of size and strain broadening to facilitate the development of the IPF. Both Type A, statistical, and Type B, systematic, uncertainties have been assigned to yield a certified value and 95% confidence uncertainty for the lattice parameter of $a = 0.415\ 682\ 6 \pm 0.000\ 008$ nm at 22.5 °C.

ACKNOWLEDGEMENTS

The use of the Advanced Photon Source at Argonne National Laboratory was supported by the U.S. Department of Energy, Office of Science, Office of Basic Energy Sciences, under Contract No. DE-AC02-06CH11357. We thank Mr. Jeff Krzywon for help in obtaining the SANS data.

Bergmann, J., Kleeberg, R., Haase, A., and Breidenstein, B. (**2000**). "Advanced fundamental parameters model for improved profile analysis," in *Proceedings of the 5th European Conference on Residual Stresses*, Vol. 347–349, edited by A. J. Böttger, R. Delhez, and E. J. Mittemeijer (Trans Tech Publications, Delft-Noordwijkerhout, The Netherlands), pp. 303–308.

BIPM (**2006**). "International System of Units (SI)," Bureau International des Poids et Mesures. Available at: https://www.bipm.org/utils/common/pdf/si_brochure_8_en.pdf (accessed August 2019).

Bruker (**2017**). *TOPAS*. Version 6 (Bruker AXS GmbH, Karlsruhe, Germany).

Cheary, R. W. and Coelho, A. A. (**1992**). "A fundamental parameters approach to X-ray line-profile fitting," J. Appl. Crystallogr. **25**, 109–121.

Cheary, R. W. and Coelho, A. A. (**1998a**). "Axial divergence in a conventional X-ray powder diffractometer I. Theoretical foundations," J. Appl. Crystallogr. **31**, 851–861.

Cheary, R. W. and Coelho, A. A. (**1998b**). "Axial divergence in a conventional X-ray powder diffractometer II. Implementation and comparison with experiment," J. Appl. Crystallogr. **31**, 862–868.

Cline, J. P., Mendenhall, M. H., Black, D., Windover, D., and Henins, A. (**2015**). "The optics, alignment and calibration of laboratory X-ray powder diffraction equipment with the use of NIST standard reference materials," J. Res. Natl. Inst. Stand. Technol. **120**, 173–222.

Cline, J. P., Mendenhall, M. H.Black, D., Windover, D., and Henins, A. (**2019**). "The optics and alignment of the divergent-beam laboratory X-ray powder diffractometer and its calibration using NIST Standard Reference Materials," in *International Tables for Crystallography, Volume H: Powder Diffraction*, edited by C. J. Gilmore, J. A. Kaduk, and H. Schenk (Wiley, Hoboken, NJ), pp. 224–251..

Hölzer, G., Fritsch, M., Deutsch, M., Härtwig, J., and Förster, E. (**1997**). "$K\alpha_{1,2}$ and $K\beta_{1,3}$ X-ray emission lines of the 3d transition metals," Phys. Rev. A **56**(6), 4554–4568.

JCGM 100 (**2008**). "Guide to the expression of uncertainty in measurement" (GUM 1995 with Minor Corrections), Joint Committee for Guides in Metrology (JCGM). Available at: https://www.bipm.org/utils/common/documents/jcgm/JCGM_100_2008_E.pdf (accessed August 2019).

https://doi.org/10.1017/S0885715620000068 Published online by Cambridge University Press

Maskil, M. and Deutsch, M. (**1988**). "X-ray K alpha satellites of copper," Phys. Rev. A **38**, 3467–3472.
Mendenhall, M. H., Mullen, K., and Cline, J. P. (**2015**). "An implementation of the fundamental parameters approach for analysis of X-ray powder diffraction line profiles," J. Res. Natl. Inst. Stand. Technol. **120**, 223–251.
NCNR (**2019**). https://www.ncnr.nist.gov/resources/activation/ (accessed December 2019).
Pawley, G. S. (**1981**). "Unit-cell refinement from powder diffraction scans," J. Appl. Cryst. **14**, 357–361.
Sirota, N. N., Novikov, V. V., Vinokrov, V. A., and Paderno, Y. B. (**1998**). "Temperature dependence of heat capacity and lattice constant of lanthanum and samarium hexaborides," Phys. Solid State **40**(11), 1856–1858.
Taylor, B. N. and Kuyatt, C. E. (**1994**). "Guidelines for evaluating and expressing the uncertainty of NIST measurement results," NIST Technical Note 1297; U.S. Government Printing Office (Washington, DC). Available at: https://www.nist.gov/pml/nist-technical-note-1297 (accessed August 2019).
Wang, J., Toby, B. H., Lee, P. L., Ribaud, L., Antao, S. M., Kurtz, C., Ramanathan, M., Von Dreele, R. B., and Beno, M. A. (**2008**). "A dedicated powder diffraction beamline at the Advanced Photon Source: commissioning and early operational results," Rev. Sci. Instrum. **79**, 085105.

https://doi.org/10.1017/S0885715620000068 Published online by Cambridge University Press